Computers and Concrete, Vol. 4, No. 5 (2007) 377-402
DOI: http://dx.doi.org/10.12989/cac.2007.4.5.377

Simulations of spacing of localized zones in reinforced concrete beams using elasto-plasticity and damage mechanics with non-local softening

I. Marzec†, J. Bobiński‡ and J. Tejchman‡†

Gdansk University of Technology Faculty of Civil and Environmental Engineering 80-952 Gdansk, Poland

(Received November 15, 2006, Accepted September 7, 2007)

Abstract. The paper presents quasi-static plane strain FE-simulations of strain localization in reinforced concrete beams without stirrups. The material was modeled with two different isotropic continuum crack models: an elasto-plastic and a damage one. In case of elasto-plasticity, linear Drucker-Prager criterion with a non-associated flow rule was defined in the compressive regime and a Rankine criterion with an associated flow rule was adopted in the tensile regime. In the case of a damage model, the degradation of the material due to micro-cracking was described with a single scalar damage parameter. To ensure the mesh-independence and to capture size effects, both criteria were enhanced in a softening regime by non-local terms. Thus, a characteristic length of micro-structure was included. The effect of a characteristic length, reinforcement ratio, bond-slip stiffness, fracture energy and beam size on strain localization was investigated. The numerical results with reinforced concrete beams were quantitatively compared with corresponding laboratory tests by Walraven (1978).

Keywords: bond-slip; concrete; characteristic length; damage mechanics; elasto-plasticity; nonlocal theory; reinforcement; strain localization.

1. Introduction

The analysis of reinforced concrete elements is complex due to occurrence of strain localization in concrete. The strain localization which is a fundamental phenomenon in concrete under both quasi-static and dynamic conditions (Bazant 1986, Wittmann, *et al.* 1992, van Vliet and van Mier 1996) can occur in the form of cracks (if cohesive properties are dominant) or shear zones (if frictional properties prevail). The determination of the width and spacing of strain localization is crucial to evaluate the material strength at peak and in the post-peak regime. The concrete behaviour can be modeled with continuum models, e.g.: non-linear elasticity (Palaniswamy and Shah 1974), fracture (Bazant and Cedolin 1979), endochronic theory (Bazant and Bhat 1976), microplane theory (Bazant and Ozbolt 1990), plasticity (Pietruszczak, *et al.* 1988, Menetrey and Willam 1995, Majewski, *et al.* 2007), damage (Dragon and Mróz 1979, Peerlings, *et al.* 1998), coupled plastic-damage (Lemaitre 1985, Salari, *et al.* 2004, Bobiński and Tejchman 2006b), and discrete ones using a lattice approach (Vervuurt, *et al.* 1994, Cusatis, *et al.* 2003, Kozicki and Tejchman 2007a) or DEM (Donze, *at al.*

†E-mail: irek@pg.gda.pl
‡E-mail: bobin@pg.gda.pl
‡†Corresponding Author, E-amil: tejchmk@pg.gda.pl

1999, D'Addetta, *et al.* 2002). To describe properly strain localization within continuum mechanics, the models should be enhanced by a characteristic length of micro-structure (Sluys 1992). There are several approaches within continuum mechanics to include a characteristic length and to preserve the well-posedness of the underlying incremental boundary value problem (de Borst, *et al.* 1992) in engineering materials as: second-gradient (Pamin 1994, Pamin and de Borst 1998), micro-polar (Mühlhaus 1986, Tejchman and Wu 1993, Tejchman, *et al.* 1999), non-local (Pijaudier-Cabot and Bazant 1987, Bobiński and Tejchman 2004) and viscous ones (Needdleman 1988, Sluys and de Borst 1996). Thus, objective and properly convergent numerical solutions for localized deformation (mesh-insensitive load-displacement diagram and mesh-insensitive deformation pattern) are achieved. Otherwise, FE-results are completely controlled by the size and orientation of the mesh and thus produce unreliable results, i.e., localized zone becomes narrower upon mesh refinement (element size becomes the characteristic length) and computed force-displacement curves change considerably depending on the width of the calculated localized zone. In addition, a premature divergence of incremental FE-calculations is often met. The presence of the characteristic length allows us to take into account inhomogeneities triggering strain localization (e.g. size and spacing of micro-defects, aggregate size, fiber spacing) and to describe a size effect (dependence of strength and other mechanical properties on the size of the specimen) observed experimentally on brittle specimens.

Other numerical technique which enables to remedy the drawbacks of standard FE-methods and to obtain mesh-independent results during the description of strain localization is the so-called strong discontinuity approach which allows a finite element with a displacement discontinuity (Simone and Sluys 2004). The approach describes softening by a traction-separation law which relates the traction transmitted by the crack to the crack opening.

In a first step, a careful FE-analysis of a deterministic size effect (caused by strain localization) in three reinforced concrete beams of a different size without shear reinforcement with two simple isotropic continuum crack models was performed. The calculations were carried out with an elasto-plastic constitutive law using a linear Drucker-Prager criterion with a non-associated flow rule in a compressive regime and a Rankine criterion with an associated flow rule in a tensile regime. In addition, the FE-calculations were performed with a damage mechanics model. To preserve the well-posedness of the boundary value problem (de Borst, *et al.* 1992), to obtain mesh-independent results, to take into account microscopic inhomogeneities triggering strain localization (e.g. aggregate size) and to include a characteristic length of micro-structure, a non-local theory was used in a softening regime as a regularization technique (Pijaudier-Cabot and Bazant 1987). The presence of a characteristic length allows also to take into account a deterministic size effect, i.e., dependence of strength and other mechanical properties on the size of the specimen. This is made possible since the ratio l_c/D governs the response of the model (l_c – characteristic length, D – specimen size). The simulations of the spacing of localized zones in reinforced concrete beams were performed with a different characteristic length of micro-structure, reinforcement ratio, fracture energy, bond-slip stiffness between concrete and reinforcement and beam size. The numerical results were directly compared with corresponding laboratory tests by Walraven (1978). A realistic determination of localized zones (width and spacing) with a continuum model is important since initially cracks have a continuous character (later they change into a discontinuous mode). A similar continuum FE-calculation was performed by Pamin and de Borst (1998) using a second gradient-enhanced crack model for one beam. In our calculations, two different continuum crack models were compared, significantly finer FE-meshes were used and the calculations were performed for 3 different beam sizes. For the sake of simplicity, plane strain conditions were assumed in beams. This assumption is justified for a large size beam since the yield stress in the reinforcement has not been reached in experiments (Walraven 1978). Moreover, the spacing of localized zone is not influenced by the assumed conditions (plane strain or plane stress) (Malecki, *et al.* 2007).

The present paper is a continuation of numerical studies of strain localization in a reinforced concrete bar under tension with a similar elasto-plastic model with non-local softening (Malecki, *et al.* 2007). The FE-simulations with a reinforced concrete bar under tension (Malecki, *et al.* 2007) showed that the width of localized zone at the residual state increased strongly with increasing characteristic length l_c and increased insignificantly with initial bond stiffness. It did not depend on the reinforcement ratio, type of the softening curve (linear or exponential) and Gaussian distribution of the tensile strength. The spacing of localized zones increased with increasing characteristic length l_c and tensile softening modulus, and decreasing reinforcement ratio, fracture energy and initial bond stiffness. It did not vary with a stochastic distribution of the tensile strength (using a usual Gaussian distribution). The width and spacing of localized zones were similar for perfect bond and usual bond-slip laws. However, localized zones occurred later for perfect bond.

2. Constitutive models for concrete

2.1. Elasto-plastic model

To describe the behaviour of a quasi-brittle material like concrete, a simplified elasto-plastic model was assumed. In the compression regime, a shear yield surface based on a linear Drucker-Prager criterion and isotropic hardening and softening was used:

$$f_1 = q + p\tan\varphi - \left(1 - \frac{1}{3}\tan\varphi\right)\sigma_c(\kappa_1) \tag{1}$$

where q - Mises equivalent deviatioric stress, p – mean stress and φ – internal friction angle. The material hardening (softening) was defined by the uniaxial compression stress $\sigma_c(\kappa_1)$, wherein κ_1 is the hardening-softening parameter corresponding to the plastic normal strain during uniaxial compression. The friction angle φ was assumed as (Abaqus 1998):

$$\tan\varphi = \frac{3(1 - r_{bc}^{\sigma})}{1 - 2r_{bc}^{\sigma}} \tag{2}$$

wherein r_{bc}^{σ} denotes the ratio between the uniaxial compression strength and biaxial compression strength (r_{bc}^{σ}=1.2). The invariants q and p were defined as

$$q = \sqrt{\frac{3}{2}s_{ij}s_{ij}}, \qquad p = \frac{1}{3}(\sigma_{kk}) \tag{3}$$

where σ_{ij} is the stress tensor and s_{ij} denotes the deviatoric stress tensor. The flow potential was assumed as

$$g_1 = q + p\tan\psi \tag{4}$$

where ψ is the dilatancy angle ($\psi \neq \varphi$). The increments of plastic strains $d\varepsilon_{ij}^{p}$ were calculated as

$$d\varepsilon_{ij}^{p} = \frac{d\kappa_1}{1-\frac{1}{3}\tan\psi}\frac{\partial g_1}{\partial\sigma_{ij}} = \frac{d\kappa_1}{1-\frac{1}{3}\tan\psi}\left(\frac{\partial q}{\partial\sigma_{ij}} + \tan\psi\frac{\partial p}{\partial\sigma_{ij}}\right) \tag{5}$$

In turn, in the tensile regime, a Rankine criterion was used with a yield function f_2 with isotropic hardening and softening defined as

$$f_2 = \max\{\sigma_1, \sigma_2, \sigma_3\} - \sigma_t(\kappa_2) \tag{6}$$

where σ_i – principal stresses, σ_t – tensile stress and κ_2 – softening parameter (equal to the maximum principal plastic strain ε_1^p). The associate flow rule was assumed. The edge and vertex in the Rankine yield function was taken into account by the interpolation of 2-3 plastic multipliers according to the Koiter's rule. The same procedure was adopted in the case of combined tension (Rankine criterion) and compression (Drucker-Prager criterion).

This simple isotropic elasto-plastic model for concrete (Eqs.1-6) requires two elastic parameters: modulus of elasticity E and Poisson's ratio ν, one compresion plastic function $\sigma_c = f(\kappa_1)$, one tensile plastic function $\sigma_t = f(\kappa_2)$, internal friction angle φ and dilatancy angle ψ. The disadvantages of the model are the following: the shape of the failure surface in a principal stress space is conical (not paraboloidal as in reality). In deviatoric planes, the shape is circular (during compression) and triangular (during tension); thus it does not change from a curvilinear triangle with smoothly rounded corners to nearly circular with increasing hydrostatic pressure. The tensile and compressive meridians of the failure surface are the same, and the stiffness degradation due to strain localization and non-linear volume changes during loading are not taken into account.

2.2. Damage model

The damage variable associated with a degradation of the material due to the propagation and coalescence of micro-cracks and micro-voids was defined as the ratio between the damage area and the overall material area (Kachanov 1986, Simo and Ju 1987). The simplest isotropic damage continuum model describes the degradation with the aid of only a single scalar damage parameter D growing monotonically from zero (undamaged material) to one (completely damaged material). The stress-strain function was represented by the following relationship

$$\sigma_{ij} = (1-D)C_{ijkl}^{e}\,\varepsilon_{kl} \tag{7}$$

where C_{ijkl}^{e} – linear elastic material stiffness matrix and ε_{kl} – strain tensor. The damage parameter D acts as a stiffness reduction factor (the Poisson ratio ν is not affected by damage). A general isotropic damage model should take into account two scalar parameters corresponding to two independent elastic constants. The growth of the damage variable D was controlled by a damage threshold parameter κ which was defined as a maximum of the equivalent strain measure ε reached during the load history up to time t. The loading function of damage was

$$f(\tilde{\varepsilon}, \kappa) = \tilde{\varepsilon} - \max\{\kappa, \kappa_0\} \tag{8}$$

where κ_0 – initial value of κ when damage begins. If the loading function f was negative, damage did not develop. During monotonic loading, the parameter κ grew (it coincided with $\tilde{\varepsilon}$) and during unloading and reloading it remained constant. To define the equivalent strain measure $\tilde{\varepsilon}$, Rankine failure type criterion (Jirasek and Marfia 2005) was assumed.

$$\tilde{\varepsilon} = \frac{1}{E}\max\{\sigma_i^{eff}\} \tag{9}$$

where E denotes the modulus of elasticity and σ_i^{eff} are the principal values of the effective stress

$$\sigma_{ij}^{eff} = C_{ijkl}^{e}\varepsilon_{kl} \tag{10}$$

To describe the evolution of the damage parameter D, an exponential softening law was used (Peerlings, *et al.* 1998)

$$D = 1 - \frac{\kappa}{\kappa_0}(1 - \alpha + \alpha e^{-\beta(\kappa - \kappa_0)}) \tag{11}$$

where α and β are the material parameters.

The constitutive isotropic damage model for concrete requires the following parameters: E, ν, κ_0, α and β. The model is suitable for tensile failure and cannot describe irreversible deformations. It cannot also realistically describe volume changes (Simone and Sluys 2004).

3. Non-local approach

To describe properly strain localization, to preserve the well-posedness of the boundary value problem, to obtain FE-results free from spurious discretization sensitivity and to capture a deterministic size effect, a integral-type non-local theory was used as a regularization technique (Pijaudier-Cabot and Bazant 1987, Bazant and Jirasek 2002) which achieves this by weighted spatial averaging of a neighborhood of each material point of a suitable state variable. A principle of a local action does not hold any more. Thus, stress at a certain material point depends not only on the state variable at that point but on the distribution of state variables in a finite neighborhood of the point considered (the principle of a local action does not hold – the non-local interaction takes place between any two points). Elasto-plastic models of this kind were developed e.g., by Brinkgreve (1994) and Bazant and Jirasek (2002). Usually, it is sufficient to treat non-locally only one variable controlling material softening or degradation (Brinkgreve 1994, Bobiński and Tejchman 2004) (whereas stresses and strains remain local).

Initially, in the calculations, the softening parameters κ_i (i=1,2) were assumed to be non-local:

$$\bar{\kappa}_i(\boldsymbol{x}) = \frac{\int_V \omega(\|\boldsymbol{x}-\xi\|)\kappa_i(\xi)\mathrm{d}\xi}{\int_V \omega(\|\boldsymbol{x}-\xi\|)\mathrm{d}\xi} \qquad \text{with } i=1, 2 \tag{12}$$

where $\bar{\kappa}_i(\boldsymbol{x})$ is the non-local softening parameter, V – the volume of the body, $\boldsymbol{x}$ – the coordinates of the considered (actual) point, ξ – the coordinates of the surrounding points and ω denotes the weighting function. In general, it is required that the weighting function should not alter a uniform field which means that it must satisfy the normalizing condition (Bazant and Jirasek 2002). Therefore, as a weighting function ω in Eq. (12), a Gauss distribution function was used for 2D-problems:

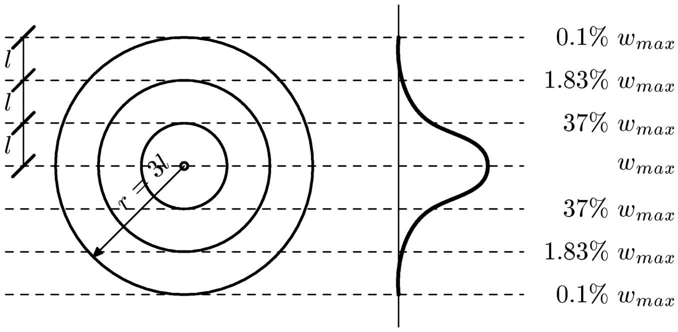

Fig. 1 Region of the influence of characteristic length l_c and weighting function ω

$$\omega(r) = \frac{1}{l_c\sqrt{\pi}} e^{-\left(\frac{r}{l_c}\right)^2} \tag{13}$$

The averaging in Eq. (13) is restricted to a small representative area around each material point (the influence of points at the distance of $r = 3l_c$ is only of 0.1%) (Fig. 1). The characteristic length can be related to the micro-structure of the material (e.g. aggregate size in concrete). According to Pijaudier-Cabot and Bazant (1987), it is in concrete approximately $3 \times d_a$, where d_a is the maximum aggregate size. It is usually determined with an inverse identification process of experimental data (Geers *et al.* 1996, Mahnken and Kuhl 1999) since it cannot be directly measured. Recently, Le Bellego *et al.* (2003) presented a calibration method of non-local models containing a characteristic length on the basis of 3 size effect bending tests. However, the determination of one representative characteristic length of micro-structure is very complex in concrete since strain localization can include a mixed mode (cracks and shear zones, Bazant and Jirasek 2002), a characteristic length is one-dimensional but is related to the fracture process zone with a certain area or volume (Bazant and Jirasek 2002) which increases during deformation (e.g. on the basis of acoustic emission measurements by Pijaudier-Cabot, *et al.* 2004). In turn, other researchers conclude that the characteristic length is not a constant, and it depends on the type of the boundary value problem and the current level of damage (Ferrara and di Prisco 2001). Thus, a determination of l_c requires further numerical analyses and measurements, e.g., using a DIC technique (Kozicki and Tejchman 2007b). In particular, the measurements of load-displacement curves and widths of the fracture process zone in experiments with the same concrete, different boundary value problems and specimen sizes are of importance.

The FE-calculations show that a classical non-local assumption (Eq.12), does not fully regularize a boundary value problem in elasto-plasticity (Brinkgreve 1994, Bobiński and Tejchman 2004). Therefore, a modified formula (according to Brinkgreve 1994) was used to calculate the rate of the non-local softening parameter:

$$\bar{\kappa}_i(\boldsymbol{x}) = (1-m)\,\kappa_i(\boldsymbol{x}) + m\frac{\int_V \omega(\|\boldsymbol{x}-\xi\|)\,\kappa_i(\xi)\mathrm{d}\xi}{\int_V \omega(\|\boldsymbol{x}-\xi\|)\mathrm{d}\xi} \qquad i = 1,2 \tag{14}$$

where m denotes a non-local parameter controlling the size of the localized plastic zone and the distribution of the plastic strain. For $m = 0$, a local approach is obtained and for $m = 1$, a classical non-local model is recovered. If the non-local parameter $m > 1$, the influence of non-locality increases and the localized plastic region reaches a finite mesh-independent size (Bobiński and Tejchman 2004). Brinkgreve (1994) derived an analytical formula for the thickness of a localized zone in an one-dimensional bar during tension with necking using a modified non-local approach by Eq. (14). According to this formula, if the parameter $m = 1$, the thickness of the localized zone was equal to zero (similarly as in a local approach). Eq. (14) can be rewritten as:

$$\bar{\kappa}_i(\boldsymbol{x}) = \kappa_i(\boldsymbol{x}) + m\left(\frac{\int_V \omega(\|\boldsymbol{x}-\xi\|)\kappa_i(\xi)\mathrm{d}\xi}{\int_V \omega(\|\boldsymbol{x}-\xi\|)\mathrm{d}\xi} - \kappa(x)\right) \qquad \text{with } i=1,2 \tag{15}$$

Since the increments of the softening parameter are not known at the beginning of each iteration, the extra sub-iterations are required to solve Eq. (15) (Strömberg and Ristinmaa 1996). To simplify the calculations, the non-local increments was replaced by their approximation $\Delta\kappa_i^{est}$ calculated on the basis of the known total strain increments (Brinkgreve 1994):

$$\Delta\bar{\kappa}_i(\boldsymbol{x}) \approx \Delta\kappa_i(\boldsymbol{x}) + m\left(\frac{\int_V \omega(\|\boldsymbol{x}-\xi\|)\Delta\kappa_i^{est}(\xi)\mathrm{d}\xi}{\int_V \omega(\|\boldsymbol{x}-\xi\|)\mathrm{d}\xi} - \Delta\kappa_i^{est}(\boldsymbol{x})\right) \quad \text{with } i=1,2 \tag{16}$$

For the Drucker-Prager and Rankine criteria, the quantities $\Delta\kappa_1^{est}$ and $\Delta\kappa_2^{est}$ were calculated according to the formulae

$$\Delta\kappa_1^{est}(\boldsymbol{x}) = \left(1 - \frac{1}{3}\tan\psi\right)\sqrt{\frac{2}{3}\Delta e_{ij}(\boldsymbol{x})\Delta e_{ij}(\boldsymbol{x})} \quad \text{and} \quad \Delta\kappa_2^{est}(\boldsymbol{x}) = \Delta\varepsilon_1(\boldsymbol{x}) \tag{17}$$

where Δe_{ij} is the total deviatoric strain increment tensor and $\Delta\varepsilon_1$ denotes the maximum principal value of the total strain increment tensor. Eq. (16) enables to 'freeze' the non-local influence of the neighboring points and to determine the actual values of the softening parameters using the same procedures as in a local formulation.

In the damage mechanics model, the equivalent strain measure $\tilde{\varepsilon}$ was replaced by its non-local definition $\bar{\varepsilon}$ (Pijaudier-Cabot and Bazant 1987)

$$\bar{\varepsilon}(x) = \frac{\int_V \omega(\|\boldsymbol{x}-\xi\|)\tilde{\varepsilon}(\xi)\mathrm{d}\xi}{\int_V \omega(\|\boldsymbol{x}-\xi\|)\mathrm{d}\xi} \tag{18}$$

to evaluate the loading function (Eq. 8) and to calculate the damage threshold parameter κ. In the elastic range, the material response was local.

The 2D and 3D non-local model was implemented in the commercial finite element code Abaqus (1998) with the aid of the subroutine UMAT (user constitutive law definition) and UEL (user element definition) for efficient computations (Bobiński and Tejchman 2004). For the solution of the non-linear equation of motion governing the response of a system of finite elements, the initial stiffness method was used with a symmetric elastic global stiffness matrix. The calculations with a full Newton-Raphson method resulted in a poor convergence in the softening regime due to the fact that the determination of the tangent stiffness matrix within a non-local theory is impossible (due to difficulties to calculate the derivatives of stresses with respect to non-local deformations). The following convergence criteria were assumed (Abaqus 1998):

$$r_{\max} \le 0.01\tilde{q} \quad \text{and} \quad c_{\max} \le 0.01\Delta u_{\max} \tag{19}$$

where $r_{\max}$ - the largest residual out-of-balance force, $\tilde{q}$ - spatially averaged force over the entire body, $c_{\max}$ – the largest correction of the displacement between two consecutive iterations and $\Delta u_{\max}$ – the largest change of the displacement in the increment. The magnitude of the maximum out-of-balance force at the end of each calculation step was smaller than 1% of the calculated total force on the specimen. The calculations with smaller tolerances did not influence the FE-results. The integration was performed at one integration point of each element (centroid).

To satisfy the consistency condition $f = 0$, if the Drucker-Prager and Rankine criterion were separately activated, the trial stress method (linearised expansion of the yield condition about the trial stress point) using an elastic predictor and a plastic corrector with the return mapping algorithm (Ortiz and Simo 1986) was applied with the following criterion:

$$[f_i / \sigma_i^{\max}] \le 10^{-6}, \qquad i=1, 2 \tag{20}$$

where $\sigma_i^{\max}$ denotes the maximum yield stress in each increment. In the case of combined tension and compression (when both criteria were simultaneously activated), the closest point projection algorithm (Abaqus 1998) was used to satisfy the consistency condition. The lack of smoothness at the edges between the different yield surfaces did not cause any numerical problems.

The calculations were carried out using a large-displacement analysis available in the Abaqus finite element code (1998). In this method, the current configuration of the body was taken into account. The Cauchy stress was taken as the stress measure. The conjugate strain rate was the rate of deformation. The rotation of the stress and strain tensor was calculated with the Hughes-Winget method (Hughes and Winget 1980). The non-local averaging was performed in the current configuration.

4. Bond between concrete and reinforcement

Bond between concrete and reinforcement plays a crucial role in structural behaviour. It embraces 3 major mechanisms: adhesion and friction between concrete and steel surface, and the bearing of reinforcement ribs against concrete. The calculations were carried out with perfect bond and bond-slip. In the first case, the same displacements along a contact surface/line between concrete and reinforcement were assumed. In the case of bond-slip, the analyses were carried out with a relation between the bond shear stress τ_b and slip u using two different bond laws according to Dörr (1980) and den Uijl and Bigaj (1996). To consider bond-slip, an interface with a zero thickness was assumed along a contact surface/line, where a relationship between the shear traction and slip was introduced. The bond law by Dörr (1980) neglects softening and assumes a yield plateau (Fig. 2A):

$$\tau_b = f_t\left[0.5\left(\frac{u}{u_0}\right) - 4.5\left(\frac{u}{u_0}\right)^2 + 1.4\left(\frac{u}{u_0}\right)^3\right] \qquad \text{if} \quad 0 < u \le u_0 \tag{21}$$

$$\tau_b = 1.9 f_t \qquad \text{if} \quad u > u_0 \tag{22}$$

wherein the parameter f_t is the tensile strength of concrete and u_0 is the displacement at which perfect slip occurs (u_o=0.06 mm). The bond law by Uijl and Bigaj (1996) distinguishes two types of bond failures, a pull-out failure and splitting failure (Fig. 2B). For the splitting failure, the radial strains are linearly dependent on the slip, and for the pull-out failure, they are nonlinear dependent.

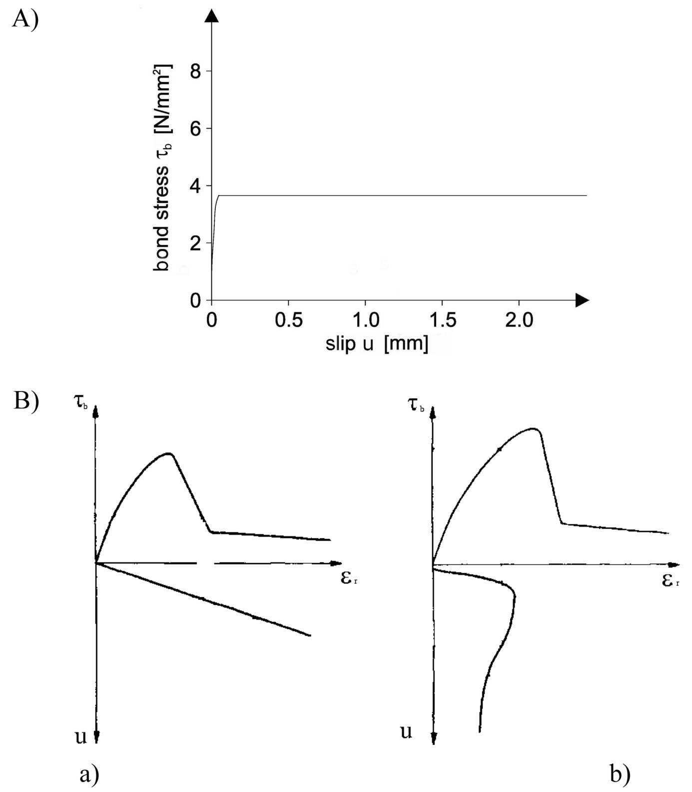

Fig. 2 Selected bond-slip laws between concrete and reinforcement: A) Dörr (1980), B) den Uijl and Bigaj (1996), a) splitting failure, b) pullout failure (τ_b – bond stress, u – slip, ε_r – radial strain)

If the radial stresses σ_r are smaller than the maximum slip stresses $\tau_b^{max} = 5f_t$, a splitting failure takes place ($\tau_b^{max}/\sigma_r > 1$), otherwise a pull-out failure takes place ($\tau_b^{max}/\sigma_r \leq 1$). A splitting failure is often caused by an insufficient concrete cover. To investigate the effect of the stiffness of the bond-slip, the tests were carried out only with the bond relation $\tau_b = f(u)$ by Dörr (1980) by changing the value of u_o.

5. Experiments on beams by Walraven (1978)

A series of tests was carried out for beams with free ends without shear reinforcement (Walraven 1978, Walraven and Lehwalter 1994). The experiments were carried out with 3 different beams with the same width of $b = 200$ mm: $h = 150$ mm, $l = 2300$ mm (small size beam '1'), $h = 450$ mm, $l = 4100$ mm (medium size beam '2') and $h = 750$ mm, $l = 6400$ mm (large size beam '3'). The average cube crushing strength of concrete was 34.2-34.8 MPa. In turn, the average cube splitting strength was 2.49-2.66 MPa. The maximum size of the aggregate in concrete was $d_a = 16$ mm. The concrete cover measured from the bar centre to the concrete surface was 25 mm (beam '1') and 30 mm (beam '2' and '3'), respectively. The effective beam height d was: $d = 125$ mm (beam '1'), $d = 420$ mm (beam '2') and $d = 720$ mm (beam '3'), respectively. The longitudinal reinforcement consisted of uncurtailed bars of deformed cold-drawn steel (with the yielding strength of 440 MPa and ratio 0.79-0.83%): $1\times\phi_s 8$ and $2\times\phi_s 10$ (beam '1'), $1\times\phi_s 20$ and $2\times\phi_s 14$ (beam '2') and $3\times\phi_s 22$ (beam '3'). The beams were incrementally loaded by two symmetric vertical forces at the distance of 1000 mm at the shear span ratio of $a/d = 3$ (a – distance between the vertical forces and beam supports: $a = 375$ mm (beam '1'), $a = 1250$ mm (beam '2') and $a = 2160$ mm (beam '3').

In all beams, the shear-tension type of failure was observed. First, vertical cracks appeared at the beginning of loading. They opened perpendicular first while later an increasing shear displacement was observed. The arising of an inclined crack led to failure. The ultimate vertical forces were: $V = 29.8$ kN (beam '1'), $V = 70.6$ kN (beam '2') and $V = 100.8$ kN (beam '3'), respectively (Figs. 5, 7 and 9). Thus, a pronounced size effect took place since the normalized shear resistance force $V_n = V/bd$ was decreasing (almost linearly) with increasing effective height d: V_n=1.26 MPa (beam '1'), $V_n = 0.84$ MPa (beam '2') and $V_n = 0.79$ MPa (beam '3'). Due to that, the cracking pattern developed significantly faster in large beams.

In the experiments, main (long) and secondary (short) cracks appeared (Figs. 6, 8 and 10). The average spacing of main and secondary cracks was: 85 mm and 65 mm (small size beam), 180 mm and 60 mm (medium size beam) and 200 mm and 85 mm (large size beam), respectively.

6. FE-model

The 2D-calculations were performed with 3 reinforced concrete beams without stirrups. 3200-22500 quadrilateral elements (composed of four diagonally crossed triangles) were used to avoid volumetric locking (Groen 1997), Fig. 3. The maximum element height, 15 mm, and element width, 23 mm, were not greater there than $3\times l_c$ (l_c = 10-30 mm) in the region of strain localization in all beams to achieve mesh-objective results.

The following elastic material parameters were assumed for concrete: $E_c = 28.9$ GPa and $\upsilon_c = 0.20$. To simplify calculations, linear relationships between the compressive σ_c and hardening (softening) parameter κ_1, and between tensile stress σ_t versus softening parameter κ_2 were assumed (Fig. 4). In the case of the tensile regime, 2 linear softening curves were assumed with κ_2^u=0.003 and κ_2^u=0.006 (κ_2^u – ultimate value of κ_2 associated with a total loss of the load bearing capacity). The internal friction angle was equal to φ = 12° (Eq. 2) and the dilatancy angle ψ= 8°. The compressive strength was equal to f_c = 34.2 MPa. The tensile strength f_t was taken from a Gaussian (normal) distribution around the mean value 2.49 MPa with a standard deviation 0.05 MPa and a cut-off ±0.1

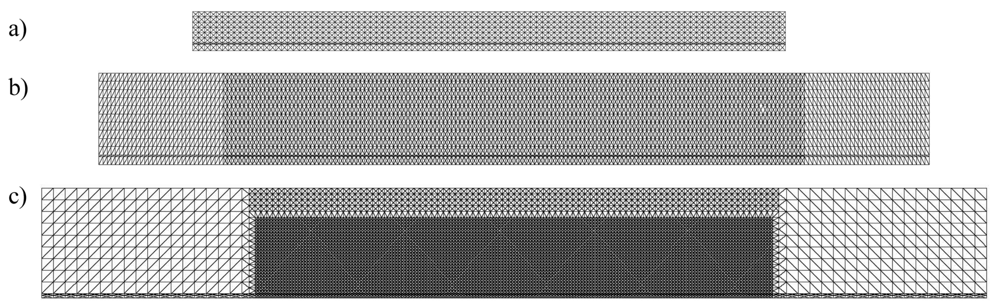

Fig. 3 FE-meshes used for calculations: a) small beam 1, b) medium beam 2, c) large beam 3 (beams are not proportionally scaled)

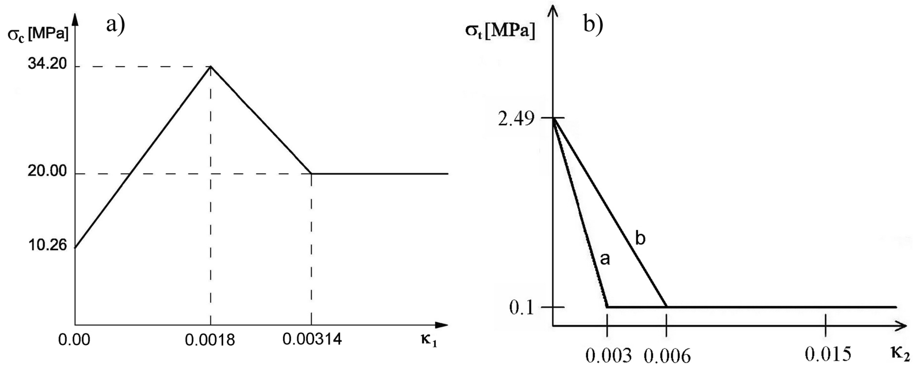

Fig. 4 Assumed curves $\sigma_c = f(\kappa_1)$ in compressive and $\sigma_t = f(\kappa_2)$ in tensile regime (σ_c – compressive stress, σ_t – tensile stress, κ_i – hardening-softening parameter)

MPa. To obtain a Gaussian distribution of the concrete strength, a polar form of the so-called Box-Muller transformation (1958) was used. The fracture energy G_f varied between 0.07 N/mm and 0.80 N/mm. It was calculated as $G_f = g_f \times w_c$; g_f – area under the softening tensile function (e.g. for linear softening $g_f = 0.5 \times f_t \times \kappa_2^u$) with $w_c \approx 3.5 \times l_c$ - crack zone width and l_c = 5-30 mm (Section 7). A characteristic length l_c was assumed in the range of l_c = 5-30 mm. The non-local parameter was chosen $m = 2$ on the basis of initial calculations (Bobiński and Tejchman 2004). In the case of the isotropic damage model, the following parameters were assumed: $\kappa_0 = 8.62 \cdot 10^{-5}$, $\alpha = 0.96$, $\beta = 200$ and l_c = 10 mm. An elasto-perfect plastic constitutive law by von Mises (Abaqus 1998) was assumed to model the reinforcement behaviour with E_s=210 GPa and σ_y=440 MPa (σ_y - yield stress). The reinforcement was assumed mainly as 2D elements. Thus, the size of these elements ($h_r \times b_r$) was 5×44 mm^2 (beam '1'), 8.8×70 mm^2 (beam '2') and 11×100 mm^2 (beam '3'). The width b_r was equal to the total perimeter of bars divided by 2 due to the contact from both sides. The calculations were carried out mainly with bond-slip (Fig. 2). The comparative calculations were also performed with reinforcement modeled as bar elements and as solid 2D-elements assuming the Poisson's ratios as υ_b=0 and υ_s=0. The reinforcement bars were fixed at ends.

7. FE-results within elasto-plasticity

7.1. Effect of a characteristic length and fracture energy

Figs. 5, 7 and 9 show the load-displacement curves for a medium, small and large size beam using the bond-slip law of Fig. 2A for different characteristic lengths (l_c = 5-30 mm) and two different fracture energies of Fig. 4(b) with $\kappa_2^u = 0.003$ and $\kappa_2^u = 0.006$ as compared to the experiments (Section 5). The reinforcement was assumed as 2D-elements. The distribution of the nonlocal parameter $\bar{\kappa}$ in the beams is depicted in Figs. 6, 8 and 10 as compared to the experimental crack distribution at the ultimate load (Walraven 1978).

The calculated load-displacements curves are in a satisfactory agreement with the experimental ones, in particular for a smaller fracture energy (κ_2^u = 0.003, $G_f \approx$ 0.13 N/mm) and a smaller characteristic length (l_c = 10 mm). The calculated ultimate vertical forces are always larger by 5-10% than the experimental ones. The bearing capacity of the beams increases with increasing l_c and

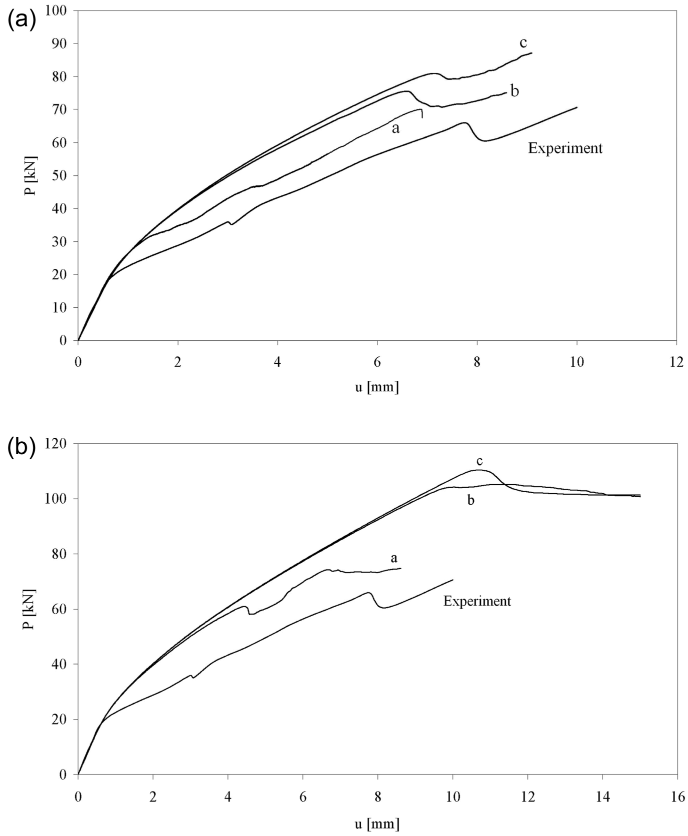

Fig. 5 Load-displacement curves for a medium size beam ($h = 450$ mm, bond-slip of Fig. 2A), $\rho = 0.75\%$, $a/d = 3$) (P – vertical resultant force, u – vertical displacement, experiment by Walraven (1978): A) $\kappa_2^u = 0.003$, B) $\kappa_2^u = 0.006$, a) $l_c = 10$ mm, b) $l_c = 20$ mm, c) $l_c = 30$ mm

fracture energy G_f. The geometry of strain localization is approximately in agreement with experiments (in particular with respect to main localized zones). There exist vertical and inclined localized zones, and long and short localized zones. The width of the localized zones is about $w_c =$ (3-4) $\times$ l_c. In turn, the calculated average spacing s of main (long) zones is approximately s = 120 mm (12 $\times$ l_c) for a small size beam, s = 190-210 mm ((7-9) $\times$ l_c) for a medium size beam and s = 190-300 mm ((15-19) $\times$ l_c) for a large size beam using model with the parameter $\kappa_2^u = 0.003$. It is s = 75-100 mm ((10-15) $\times$ l_c) for a small size beam and s = 160-210 mm ((7-16) $\times$ l_c) for a medium size beam when the parameter $\kappa_2^u = 0.006$ was used. Thus, the spacing of localized zones increases with increasing characteristic length and beam height and decreasing fracture energy. In contrast to experiments, the height of localized zones is in FE-analyses slightly smaller and the number of inclined zones is also smaller.

The FE-results for a small, medium and large size beam with reinforcement ratio $\rho = 0.75\%$, l_c = 10 mm, $\kappa_2^u = 0.003$ and reinforcement assumed as a 1D bar element are given in Figs. 11 and 12. In this case, the agreement with experimental results is even better. The calculated normalized ultimate shear are: V_n = 1.29 MPa (small size beam), V_n = 0.90 MPa (medium size beam) and V_n = 0.61 MPa (large size beam) (Fig. 11). The experimental values are V_n = 1.26 MPa (small size

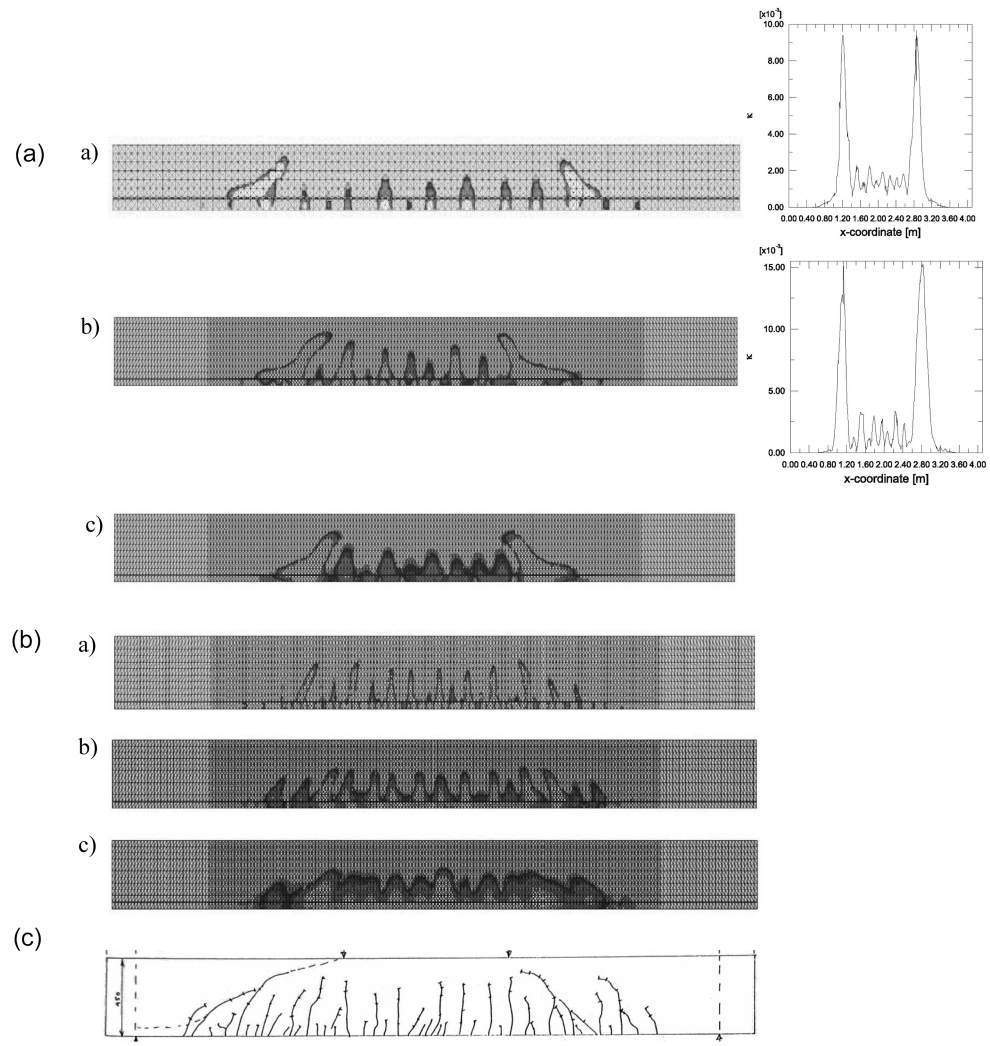

Fig. 6 Distribution of the non-local softening parameter κ_2 in a medium size beam at vertical displacement of u = 8.5 mm (h = 450 mm, bond-slip of Fig. 2A), ρ = 0.75%, a/d = 3) compared to experiments by Walraven (1978) (C): A) κ_2^u = 0.003, B) κ_2^u = 0.006, a) l_c = 10 mm, b) l_c = 20 mm, c) l_c = 30 mm

beam), V_n = 0.84 MPa (medium size beam) and V_n = 0.63 MPa (large size beam), respectively. Thus, the ultimate forces differ only by 5% for all beams. Thus, the size effect is satisfactorily reproduced in the FE-analysis. The spacing average of main localized zones (l_c = 10 mm, κ_2^u = 0.003): s = 70 mm ($7\times l_c$) (small size beam), s = 170 mm ($17 \times l_c$) (medium size beam) and s = 190 mm ($19\times l_c$) for a large size beam is also close to the experimental outcomes equal to 85 mm (small size beam), 160 mm (medium size beam) and 200 mm (large size beam), respectively. In the case of a large size beam, the spacing of all localized (main and secondary) zones, 90 mm ($19\times l_c$), is also in a good accordance with the experiment (85 mm).

The calculated spacing of fracture process zones s was also compared with the average crack spacing according to CEB-FIP Model Code (1991):

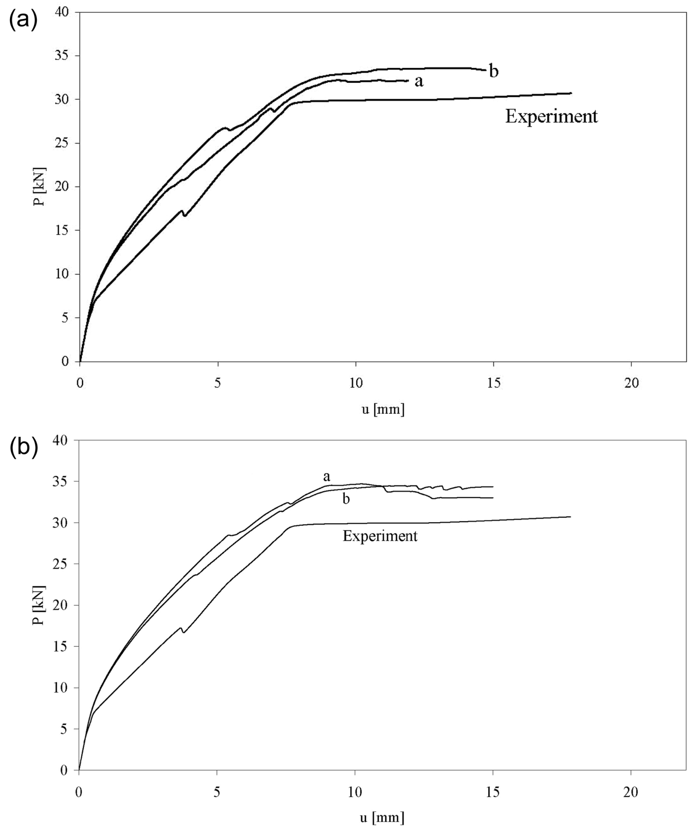

Fig. 7 Load-displacement curves for a small size beam (h = 150 mm, bond-slip of Fig. 2A, $\rho = 0.75\%$, a/d = 3) (P – vertical resultant force, u – vertical displacement, 'e' – experiment by Walraven (1978): A) κ_2^u = 0.003, B) $\kappa_2^u = 0.006$, a) $l_c = 5$ mm, b) $l_c = 10$ mm

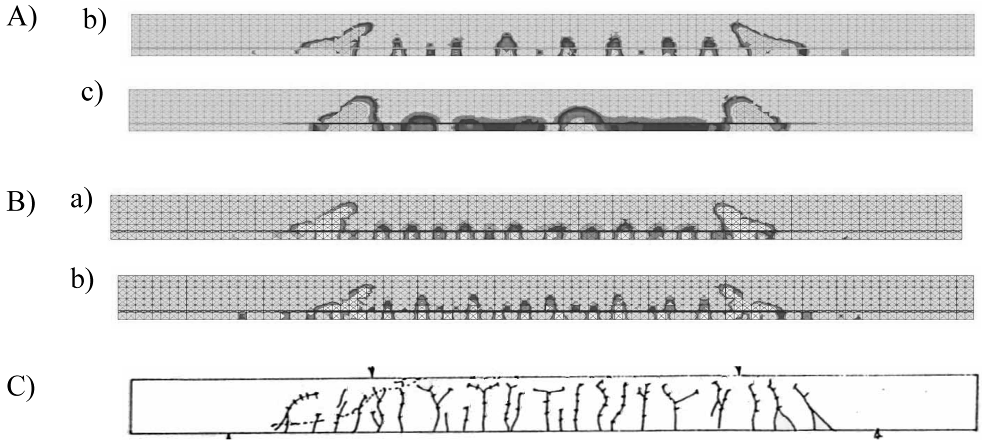

Fig. 8 Distribution of the non-local softening parameter κ_2 in a small size beam at vertical displacement of u = 8.5 mm (h = 150 mm, bond-slip of Fig. 2A), $\rho = 0.75\%$, $a/d = 3$) compared to experiments by Walraven (1978) (C): A) κ_2^u = 0.003, B) κ_2^u = 0.006, a) $l_c = 5$ mm, b) $l_c = 10$ mm, c) $l_c = 20$ mm, C) experiment

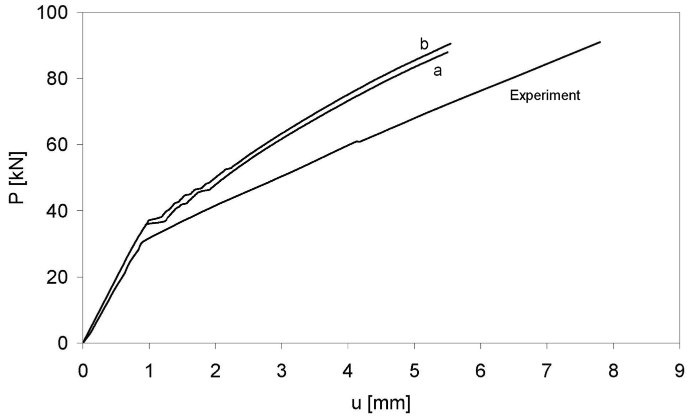

Fig. 9 Load-displacement curves for a larsge size beam (h = 750 mm, bond-slip of Fig. 2A, ρ = 0.75%, a/d = 3, κ_2^u = 0.003) (P – vertical resultant force, u – vertical displacement, experiment by Walraven (1978): a) l_c = 10 mm, b) l_c = 20 mm, c) experiment

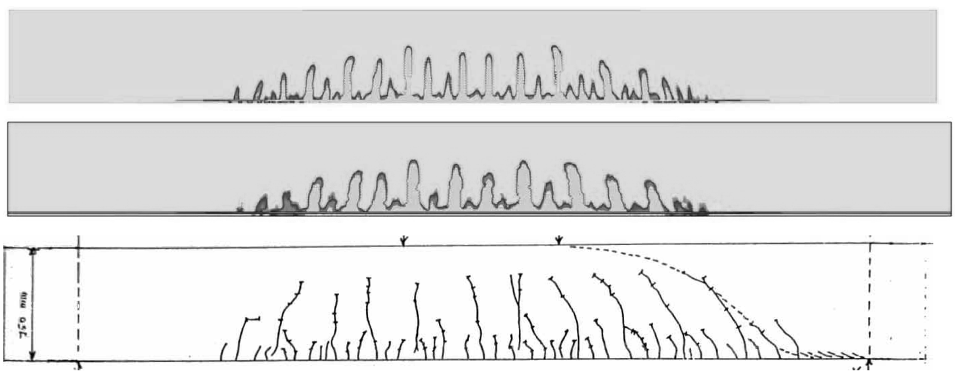

Fig. 10 Distribution of the non-local softening parameter κ_2 in a large size beam at vertical displacement of u = 8.5 mm (h = 750 mm, bond-slip of Fig. 2A), ρ = 0.75%, a/d = 3, κ_2^u = 0.003) compared to experiments by Walraven (1978): a) l_c = 10 mm, b) l_c = 20 mm, c) experiment

$$s = \frac{2}{3} \times \frac{\phi_s}{3.6\rho} = \frac{2}{3} \times \frac{9}{3.6 \times 0.0075} = 223 \text{ mm (small size beam)} \tag{23}$$

$$s = \frac{2}{3} \times \frac{\phi_s}{3.6\rho} = \frac{2}{3} \times \frac{16}{3.6 \times 0.0075} = 395 \text{ mm (medium size beam)} \tag{24}$$

$$s = \frac{2}{3} \times \frac{\phi_s}{3.6\rho} = \frac{2}{3} \times \frac{22}{3.6 \times 0.0075} = 543 \text{ mm (large size beam)} \tag{25}$$

and the formula by Lorrain, *et al.* (1998):

$$s = 1.5c + 0.1\frac{\phi_s}{\rho} = 1.5 \times 20.5 + 0.1\frac{9}{0.0075} = 150 \text{ mm (small size beam)} \tag{26}$$

$$s = 1.5c + 0.1\frac{\phi_s}{\rho} = 1.5 \times 22.0 + 0.1\frac{16}{0.0075} = 246 \text{ mm (medium size beam)} \tag{27}$$

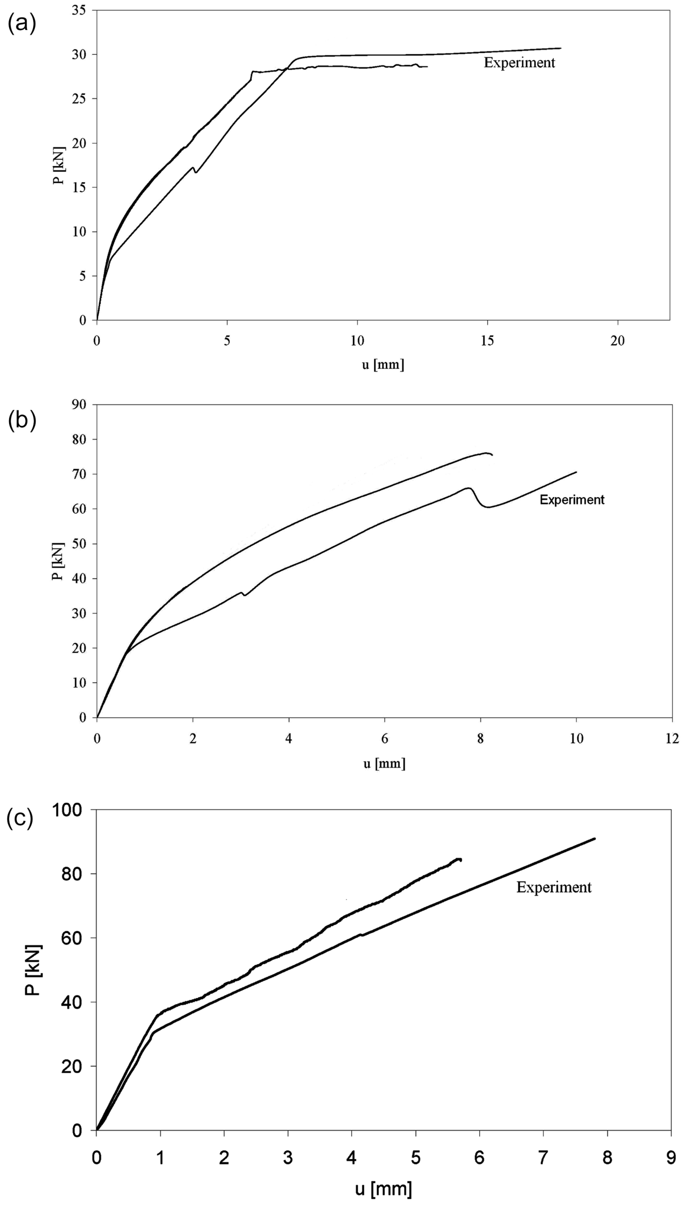

Fig. 11 Load-displacement curves (a/d = 3, ρ = 0.75%, κ_2^u = 0.003, l_c = 10 mm, bond-slip, reinforcement as 1D element): a) small beam, b) medium beam, c) large beam

$$s = 1.5c + 0.1\frac{\phi_s}{\rho} = 1.5 \times 19 + 0.1\frac{22}{0.0075} = 322 \text{ mm} \quad \text{(large size beam)} \tag{28}$$

wherein ϕ_s = 9 mm, ϕ_s = 16 mm and ϕ_s = 22 mm are the mean reinforcing bar diameters in a small, medium and large beam, ρ = 0.75% denotes the reinforcement ratio and c denotes the concrete cover. The calculated and experimental spacing of localized zones is significantly smaller than these obtained with different analytical formulas. The effect of a characteristic length and fracture energy

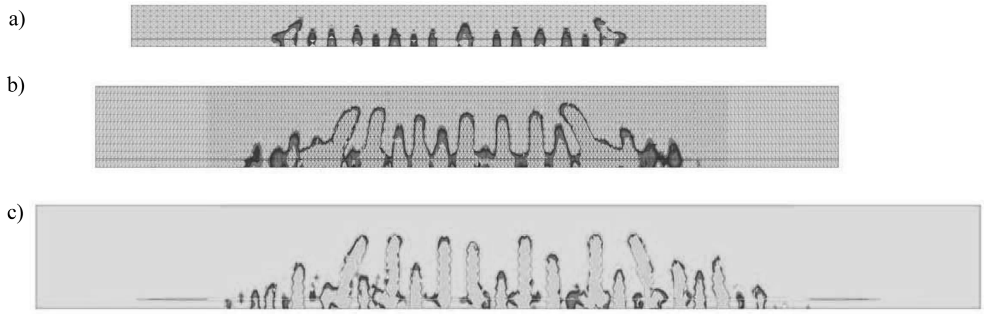

Fig. 12 Distribution of the non-local softening parameter κ_2 (a/d = 3, ρ = 0.75%, κ_2^u = 0.003, l_c = 10 mm, bond-slip, reinforcement as 1D element) in: a) small beam, b) medium beam, c) large beam

on the spacing of localized zones is similar as in the calculations of by Pamin and de Borst (1998) for a medium size beam using a second gradient-enhanced crack model with a Rankine failure surface approximated by a circular function in the tension-tension regime under plane stress conditions. The geometry of localized zones is also similar.

7.2. Effect of tensile strength f_c

The calculations were carried out with a different tensile strength f_t using a linear softening curve '*a*' of Fig. 2b (bond-slip of Fig. 2A, a/d = 3, medium beam, l_c = 20 mm, κ_2^u = 0.003, ρ = 0.75%, reinforcement as 2D elements). The tensile strength was f_t = 2.49 MPa, f_t = 2.66 MPa and f_t = 2.90 MPa, respectively. An increase of the tensile strength causes a linear increase of the ultimate shear force; from V = 75.5 kN (f_t = 2.49 MPa) and V = 77.5 kN (f_t = 2.66 MPa) up to V = 80.0 kN (f_t = 2.9 MPa). Such linear dependency is in accordance with experiments (Kani 1966).

7.3. Effect of reinforcement ratio ρ

The effect of the reinforcement ratio in a medium beam for l_c = 20 mm (using the bond-slip law of Fig. 2A and curve '*b'* of Fig. 4b) was investigated for ρ = 1.5% and ρ = 2.0%. The spacing of localized zones decreases with increasing ρ (s = 190 mm for ρ = 0.75%, s = 160 mm for ρ = 1.5% and s = 140 mm for ρ = 2.0%). The crack width is always the same (3-4) × l_c.

The calculations were also performed with the Poisson's ratios: υ_s = 0 (ρ = 0.75%) and υ_c = 0 and υ_s = 0 (ρ = 1.50%). In the first case, the ultimate shear resistance was smaller by 5% (from 70 kN down to 67 kN) and in the second case was reduced by 10% (from 119.2 kN down to 110.1 kN). The spacing of localized zones was unaffected.

7.4. Effect of shear span ratio a/d

The effect of the shear span ratio a/d in the range of a/d = 2-3.5 on the distribution of localized zones is shown in Fig. 13 for a medium beam using a bond-slip of Fig. 2A (ρ = 0.75%, l_c = 20 mm, κ_2^u = 0.003, reinforcement as 2D elements).

The ultimate shear resistance force V obviously decreases with increasing distance of vertical forces from the supports a/d (from V = 95.1 kN for a/d = 2, V = 75.5 kN for a/d = 3 down to V =

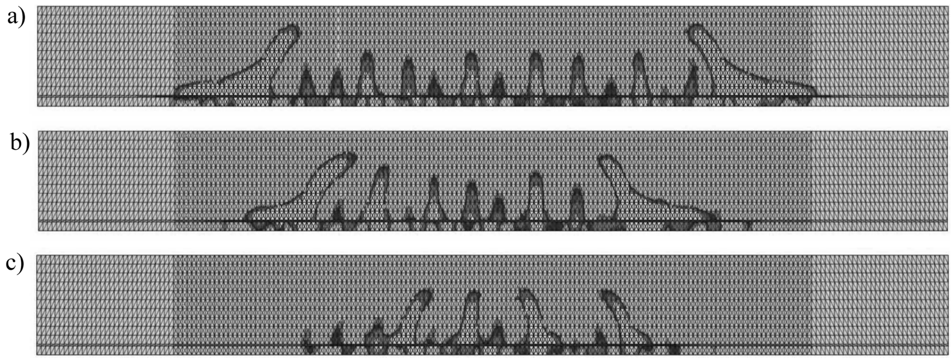

Fig. 13 Distribution of the non-local softening parameter κ_2 in a medium size beam at vertical displacement of u = 8.5 mm (bond-slip of Fig. 2A)), l_c = 20 mm, ρ = 0.75%, κ_2^u = 0.003) for different ratios a/d: a) a/d = 2, b) a/d = 3, c) a/d = 3.5

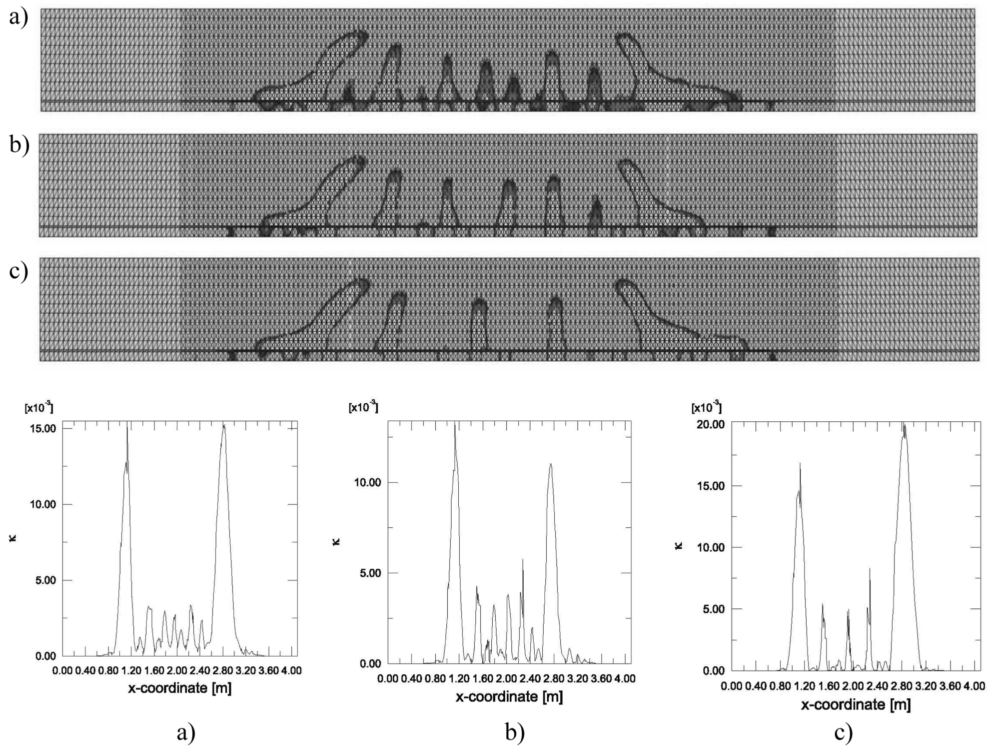

Fig. 14 Distribution of the non-local softening parameter κ_2 in a medium size beam at vertical displacement of u = 8.5 mm (bond-slip of Fig. 2A)), l_c = 20 mm, ρ = 0.75%, κ_2^u = 0.003): a) u_o = 0.06 mm, b) u_o = 0.12 mm, c) u_o = 0.24 mm

60 kN for a/d = 3.5). The dependence is parabolic which is in good agreement with experiments (Kani 1966) and calculations (Jia, *et al.* 2006)

The width of localized zones was about w = (3-4) × l_c. The spacing of localized zones slightly increases with increasing a/d (from s = 170 mm with a/d = 2, s = 190 mm with a/d = 3-3.5).

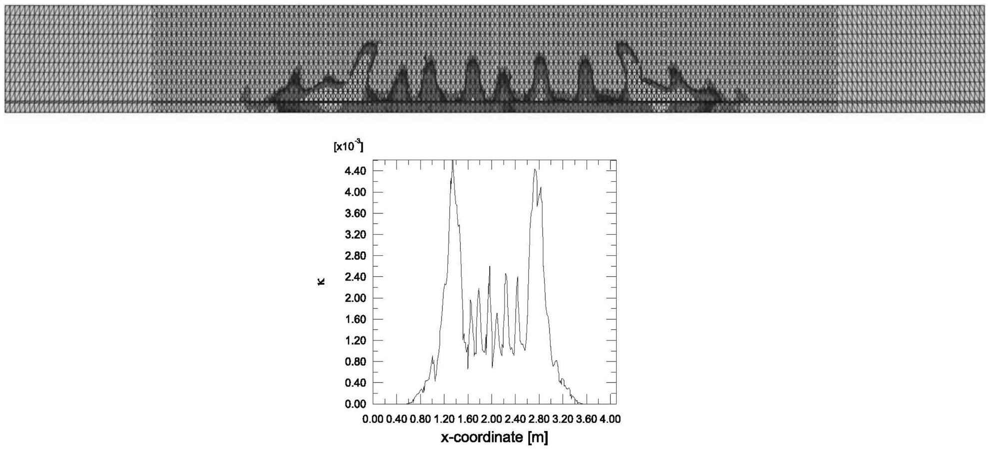

Fig. 16 Distribution of the non-local softening parameter κ_2 in a medium size beam at vertical displacement of u = 8.5 mm (perfect bond, a/d = 3, ρ = 0.75%, κ_2^u = 0.003, l_c = 20 mm)

7.5. Effect of bond-slip

The type of the bond law (Figs. 2A and 2B) insignificantly influences the load-displacement diagram and width and spacing of localized zones. Since the bond traction values are far from the limiting value (the softening part of the bond law has not been reached), the cracking process is influenced by the initial bond stiffness only. The effect of the stiffness of bond-slip of Fig. 2A (in the range of u_o = 0.06-0.24 mm) on the distribution of localized zones is shown in Fig. 14 for a medium size beam (ρ = 0.75%, l_c = 20 mm, κ_2^u = 0.003, bond-slip law of Fig. 2A).

The spacing of localized zones increases with decreasing initial bond stiffness; from s=190 mm ($12 \times l_c$) for u_o = 0.06 mm, s = 340 mm ($17 \times l_c$) for u_o = 0.12 mm up to s = 480 mm ($24 \times l_c$) for u_o = 0.24 mm. In turn, the width of localized zones decreases with decreasing initial bond stiffness from $3.5 \times l_c$ (u_o = 0.06 mm) down to $3 \times l_c$ (u_o = 0.12-0.24 mm).

Figs. 15 and 16 demonstrate the results with perfect bond (medium beam, (ρ = 0.75%, l_c = 20-30 mm, κ_2^u = 0.003). The ultimate vertical force V is larger for perfect bond by 5%. The crack spacing

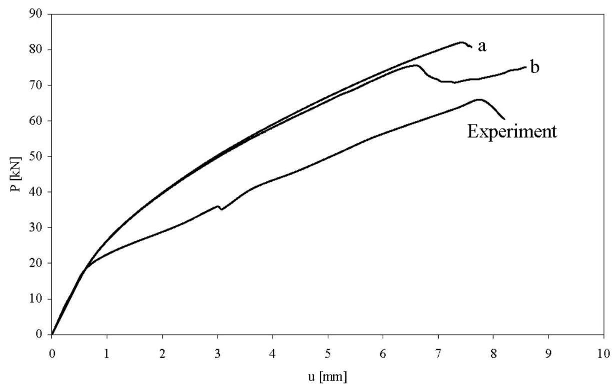

Fig. 15 Load-displacement curves for a medium size beam (a/d = 3, ρ = 0.75%, κ_2^u = 0.003, l_c = 20 mm): a) perfect bond, b) bond-slip

of localized zones is slightly smaller for perfect bond (s = 180 mm). Their width is similar.

8. FE-results within damage mechanics

Fig. 17 shows the load-displacement curves for a medium, small and large size beam using the bond-slip law of Fig. 2A for a characteristic lengths of l_c = 10 mm as compared to the experiments

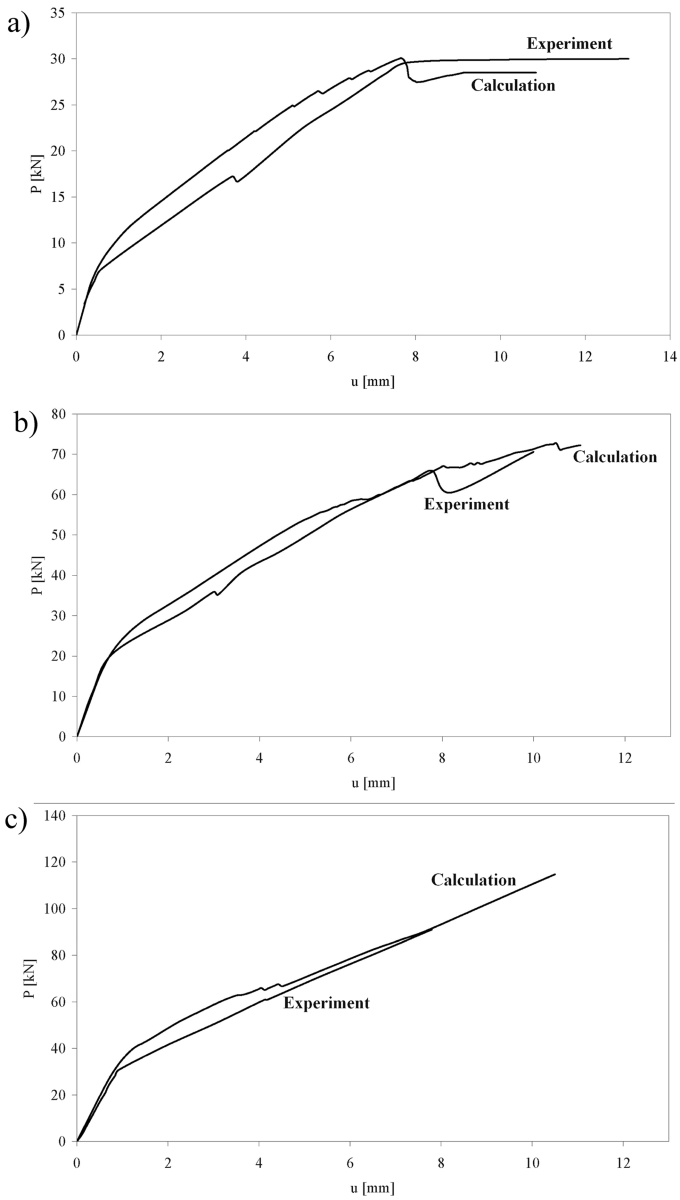

Fig. 17 Load-displacement curves (a/d = 3, ρ = 0.75%, l_c = 10 mm, bond-slip, reinforcement as 2D elements): a) small beam, b) medium beam, c) large beam (damage mechanics)

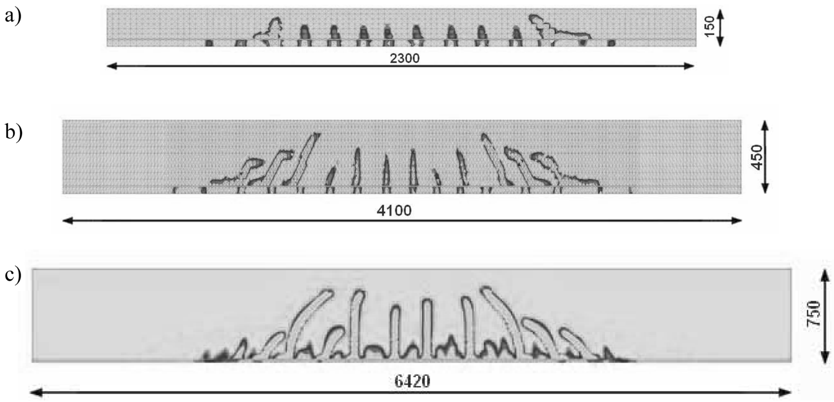

Fig. 18 Distribution of the non-local softening parameter (a/d = 3, ρ = 0.75%, l_c = 10 mm, bond-slip, reinforcement as 2D elements) in: a) small beam, b) medium beam, c) large beam (damage mechanics) (beams are not proportionally scaled)

Table 1 Description of FE-simulations

Simulation no.	Beam size	Shear span ratio a/d	Constitutive model	Softening parameter κ_u	Characteristic length l_c [mm]	Bond model
1a					10	
1b	m	3	ep	0.003	20	2D bs
1c					30	
2a					10	
2b	m	3	ep	0.006	20	2D bs
2c					30	
3a	s	3	ep	0.003	5	2D bs
3b					10	
4a	s	3	ep	0.006	5	2D bs
4b					10	
5a	l	3	ep	0.003	10	2D bs
5b					20	
6a	s					
6b	m	3	ep	0.003	10	1D bs
6c	l					
7a		2				
7b	m	3	ep	0.003	20	2D bs
7c		3.5				
8a						2D bs (u_o=0.06 mm)
8b	m	3	ep	0.003	20	2D bs (u_o=0.12 mm)
8c						2D bs (u_o=0.24 mm)

Table 1 Continued

Simulation no.	Beam size	Shear span ratio a/d	Constitutive model	Softening parameter κ_u	Characteristic length l_c [mm]	Bond model
9a 9b	m	3	ep	0.003	20	2D bs 2D pb
10a 10b 10c	s m l	3	d	-	10	2D bs

*‘s’- small size beam, ‘m’ –medium size beam, ‘l’ – large size beam
‘ep’ – elasto-plastic model, ‘d’ – damage model
‘bs’ – bond-slip, ‘pb’ – perfect bond

Table 2 Data summary of experiments (failure forces and spacing of long cracks), FE-results (corresponding failure forces and spacing of localized zones) and analytical formulae (crack spacing)

No.	Failure vertical force (experiments) [kN]	Spacing of long cracks (experiments) [mm]	Vertical force from FEM [kN]	Spacing of localized ones from FEM [mm]	Crack spacing by CEB-FIP Model (1990) [mm]	Crack spacing by Lorrain *et al.* (1998) [mm]
1a 1b 1c	70.6	180	70.1 75.5 80.6	190-210	395	246
2a 2b 2c	70.6	180	75.0 101.3 110.0	160-210	395	246
3a 3b	29.8	85	32.2 33.1	120	223	150
4a 4b	29.8	85	34.1 33.8	75-100	223	150
5a 5b	100.8	200	87.9 90.8	190-300	543	322
6a 6b 6c	29.8 70.6 100.8	85 180 200	28.1 76.0 83.4	70 170 190	223 395 543	150 246 322
7a 7b 7c	- 70.6 -	180	95.1 70.6 60.0	170-190	395	246
8a 8b 8c	70.6	180	-	190 340 480	395	246
9a 9b	70.6	180	75.5 81.3	180	395	246
10a 10b 10c	29.8 70.6 100.8	85 180 200	30.1 72.3 95.0	100 160 240	223 395 543	150 246 322

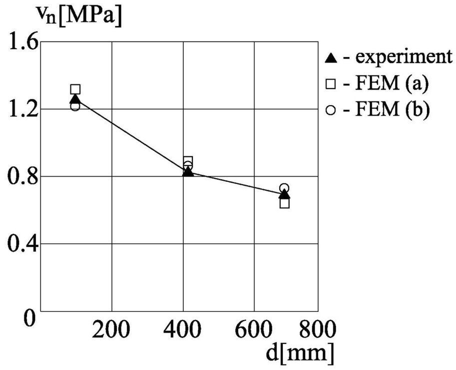

Fig. 19 Calculated size effect in reinforced concrete beams from FE-analyses as compared to experiments by Walraven (1978) (V_n - normalized shear resistance force, d - effective height, a) - elasto-plastic model, b) damage model)

(Section 5). The reinforcement was assumed as 2D-elements. The distribution of the nonlocal parameter $\bar{\varepsilon}$ (Eq. 18) in the beams is depicted in Fig. 18.

The evolution of the vertical force is similar as in the experiment (Fig. 17). The agreement with experiments is even better than within elasto-plasticity since the calculated ultimate vertical forces differ only by 3% from the experimental ones. The calculated normalized ultimate shear forces are: V_n = 1.20 MPa (small size beam), V_n = 0.86 MPa (medium size beam) and V_n = 0.64 (large size beam) respectively.

The calculated average spacing of main localized zones s is approximately s = 100 mm ($10 \times l_c$) for a small size beam, s = 160 mm ($16 \times l_c$) for a medium size beam and s = 240 mm ($24 \times l_c$) for a large size beam (Fig. 18). Thus, the spacing of localized zones is similar for a medium size beam and larger in the case of a small and large size beam as compared to elasto-plastic solutions.

The summarized description of FE-simulations is given in Table 1. Table 2 compares the experimental results with respect to failure forces and spacing of main cracks with corresponding calculated forces and calculated spacing of localized zones and analytical formulae for the crack spacing. In turn, Fig. 19 demonstrates a comparison between the calculated and experimental size effect.

9. Conclusions

The FE-simulations have shown that the isotropic elasto-plastic and damage continuum crack models with non-local softening are able to capture localized zones in a reinforced concrete beams without shear reinforcement. The FE-analyses revealed the following points:

• in spite of the simplicity of the used models, the calculated normalized material strength and spacing of main localized zones are in a satisfactory agreement with experiments. The evolution of load-displacement curves is also similar. The differences concern the length and shape of localized zones,

• the FE-results are similar within two different continuum crack models, although a slightly better agreement with experiments was achieved with a damage model,

• the beam strength increases mainly with increasing reinforcement ratio, characteristic length, tensile strength, fracture energy and decreasing beam size and shear span ratio. It is not affected by the type of the bond-slip,

• the calculated ultimate forces differ by about 5% as compared to experimental ones when $l_c =$ 10 mm. To a achieve a better agreement, the characteristic length and fracture energy should be smaller (l_c<10 mm, G_f< 0.10 N/mm). However this will be connected to a larger computation time since the size of the finite element has to be reduced with a respect to a smaller characteristic length (to obtain mesh-independent results),

• the calculated size effect is realistically captured, the bearing capacity of beams increases with decreasing beam size,

• the calculated width of primary localized zones increases strongly with increasing characteristic length l_c. The width is about (3-4) × l_c,

• the calculated spacing of primary localized zones increases with increasing characteristic length l_c, tensile softening modulus and decreasing fracture energy, reinforcement ratio and initial bond stiffness. It is not affected by the type of the bond-slip. The spacing changes from (7-10) × l_c (small size beam) and (16-17) × l_c (medium size beam) up to (19-24) × l_c (large size beam). In the case of main pronounced cracks, it is in a good agreement with experiments and is smaller than this given by different analytical formulas,

• the reinforcement can be modeled as 2D and 1D elements.

The numerical calculations of strain localization with a non-local continuum model will be continued. The 3D calculations will be carried out with reinforced concrete beams with shear reinforcement (Walraven and Lehwalter 1994) where a strong size effect was also observed. In a compressive regime, a more advanced elasto-plastic model by Menetrey and Willam (1995) will be used. A hardening elasto-plastic model will be combined with a damage model with non-local softening (Bobiński and Tejchman 2006) to capture the stiffness degradation during strain localization. Anisotropy will be included (Gatuingt 2006). To describe a statistical size effect, a spatially correlated distribution of the tensile strength will be assumed (Tejchman and Górski 2007) where choice of the representative samples will be governed by a Latin hypercube sampling method. In addition, laboratory tests will be performed wherein the width of the fracture process zone will be measured in beams using a DIC technique (Kozicki and Tejchman 2007b). Afterwards, a continuum model will be connected with a discontinuous crack type model (Simone and Sluys 2004).

Acknowledgements

The numerical calculations were performed on supercomputers of the Academic Computer Centre in Gdansk TASK.

References

Abaqus, Theory Manual, (1998), Version 5.8, Hibbit, Karlsson & Sorensen Inc.

Bazant, Z. P. and Bhat, P. D. (1976), "Endochronic theory of inelasticity and failure of concrete", *J. Eng. Mech. Div. ASCE*, **102**, 701-722.

Bazant, Z. P. and Cedolin, L. (1979), "Blunt crackband propagation in finite element analysis", *J. Eng. Mech. Div. ASCE*, 105, 2, 297-315.

Bazant, Z. and Ozbolt, J. (1990), "Non-local microplane model for fracture, damage and size effect in structures", *J. Eng. Mech. ASCE*, **116**, 2485-2505.

Bazant, Z. P. and Jirasek, M. (2002), "Nonlocal integral formulations of plasticity and damage: survey of progress", *J. Eng. Mech*. 128, 11, 1119-1149.

Bobiński, J. and Tejchman, J. (2004), "Numerical simulations of localization of deformation in quasi-brittle materials within non-local softening plasticity", *Comput. Concrete,* **4**, 433-455.
Bobiński, J. and Tejchman, J. (2006), "Modelling of strain localization in quasi-brittle materials with a coupled elasto-plastic-damage model", *Theoretical Appl. Mech.*, **44**, 767-782.
de Borst, R., Mühlhaus, H.-B, Pamin, J. and Sluys, L. (1992), "Computational modelling of localization of deformation", *Proc. of the 3rd Int. Conf. Comp. Plasticity* (eds.: D. R. J. Owen, H. Onate, E. Hinton), Swansea, Pineridge Press 483-508.
Box, G. E. P. and Muller, M. E. (1958), "A note of the generation of random normal deviates", *Annals. Math. Stat.*, **29**, 610-611, 1958.
Brinkgreve, R. B. (1994), "Geomaterial models and numerical analysis of softening", PhD thesis, Delft University of Technology, Delft.
CEB-FIP Model Code 1990 for Concrete Structures (1991), **228**, 1-205.
Cusatis, G., Bazant, Z. P. and Cedolin, L. (2003), "Confinement-shear lattice model for concrete damage in tension and compression: I. Theory", *J. Eng. Mech. ASCE,* 1439-1448.
D'Addetta, G. A., Kun, F. and Ramm, E. (2002), "In the application of a discrete model to the fracture process of cohesive granular materials", *Granular Matter,* **4**, 77-90.
Donze, F. V., Magnier, S. A., Daudeville, L., Mariotti, C. and Davenne, L. (1999), "Numerical study of compressive behaviour of concrete at high strain rates", *J. Eng. Mech.*, 1154-1163.
Dörr, K. (1980), "Ein Beitrag zur Berechnung von Stahlbetonscheiben unter besonderer Berücksichtigung des Verbundverhaltens", PhD thesis, Darmstadt University.
Dragon, A. and Mroz, Z. (1979), "A continuum model for plastic-brittle behaviour of rock and concrete", *Int. J. Eng. Sci.*, 17.
Eurocode 2 (1991), "Design of Concrete Structures, part 1-1".
Ferrara, I., di Prisco, M. (2001), "Mode I fracture behaviour in concrete: nonlocal damage modeling", *ASCE J. Eng. Mech.*, **127**(7), 678-692.
Gatuingt, F., Desmorat, R. and Ragnueneau, F. (2006). "Finite element computation of rupture with induced anisotropic damage", *Compu. Modelling of Concrete Structures, EURO-C* 2006 (eds.: G. Meschke, R. de Borst, H. Mang and N. Bicanic)*,* Taylor and Francis, 345-352.
Geers, M., Peijs, T., Brekelmans, W. and de Borst, R. (1996), "Experimental monitoring of strain localization and failure behaviour of composite materials", *Compos. Sci. Tech.*, **56**, 1283-1290.
Groen, A. E. (1997), "Three-dimensional elasto-plastic analysis of soils", *PhD Thesis*, Delft University, 1-114.
Hughes T. J. R. and Winget J. (1980), "Finite rotation effects in numerical integration of rate constitutive equations arising in large deformation analysis", *Int. J. Numer. Methods Eng.*, **15**, 1862-1867.
Jirasek, M. and Marfia, S. (2005), "Non-local damage model based on displacement averaging", *Int. J. for Numer. Meths. Eng.*, **63**, 77-102.
Kachanov, L. M. (1986), *Introduction to Continuum Damage Mechanics*, Dordrecht: Martimus Nijhoff.
Kani, G. N. J. (1966), "Basic facts concerning shear failure", *ACI-Journal Proceedings*, **63**, 675-692.
Kozicki, J. and Tejchman, J. (2007a), "Effect of aggregate structure on fracture process in concrete using 2D lattice model", *Archives of Mechanics*, 2007 (in press).
Kozicki, J. and Tejchman, J. (2007b), "Experimental investigations of strain localization in concrete using Digital Image Correlation (DIC) technique", *Archives of Hydro-Engineering and Environmental Mechanics,* 54, 1, pp.3-24.
Le Bellego, C., Dube, J. F., Pijaudier-Cabot, G. and Gerard, B. (2003), "Calibration of nonlocal damage model from size effect tests", *E. J. Mechanics A/Solids* **22**, 33-46.
Lemaitre, J. (1985), "Coupled elasto-plasticity and damage constitutive equations", *Comput Methods Appl. Mech. Eng.*, **51**, 31-49.
Lorrain, M., Maurel, O. and Seffo, M. (1998), "Cracking behaviour of reinforced high-strength concrete tension ties", *ACI Struct. J.*, **95**(5), 626-635.
Majewski, T., Bobiński, J. and Tejchman, J. (2007), "FE-analysis of failure behaviour of reinforced concrete columns under eccentric compression", *Eng. Struct.* (in press).
Mahnken, R. and Kuhl, E. (1999), "Parameter identification of gradient enhanced damage models", *Eur. J. Mech. A/Solids*, **18**, 819-835.

Malecki, T., Marzec, I., Bobiński, J. and Tejchman, J. (2007), "Effect of a characteristic length on crack spacing in a reinforced concrete bar under tension", *Mech. Res. Com.* (in press).

Menetrey, P. and Willam, K. J. (1995), "Triaxial failure criterion for concrete and its generalization", *ACI Struct. J.*, 311-318.

Mühlhaus, H.-B. (1986), "Scherfugenanalyse bei granularen material im rahmen der cosserat-theorie", *Ingenieur Archiv*, **56**, 389-399.

Needdleman, A. (1988), "Material rate dependence and mesh sensitivity in localization problems", *Comput. Methods. Appl. Mech. Eng*. **67**, 69-85.

Ortiz, M. and Simo, I. C. (1986), "An analysis of a new class of integration algorithms for elastoplastic constitutive relation", *Int. I, Num. Methods Eng*., **23**, 353-366.

Palaniswamy, R. and Shah, S. P. (1974), "Fracture and stress-strain relationship of concrete under triaxial compression", *J. Struct. Div. ASCE*, **100**, 901-916.

Pamin, J. (1994), "Gradient-dependent plasticity in numerical simulation of localization phenomena", PhD *Thesis*, University of Delft.

Pamin, J. and de Borst, R. (1998), "Simulation of crack spacing using a reinforced concrete model with an internal length parameter", *Arch. App. Mech*., **68**(9), 613-625.

Peerlings, R. H. J., de Borst, R., Brekelmans, W. A. M. and Geers, M. G. D. (1998), "Gradient enhanced damage modelling of concrete fracture", *Mech. Cohesion.-Friction. Materials*, **3**, 323-342.

Pijaudier-Cabot, G. and Bazant, Z. P. (1987), "Nonlocal damage theory", *ASCE, J. Eng. Mech.*, **113**, 1512-1533.

Pietruszczak, D., Jiang, J. and Mirza, F. A. (1988), "An elastoplastic constitutive model for concrete", *Int. J. Solids Structures*, **24**(7), 705-722.

Salari, M. R., Saeb, S., Willam, K. J., Patchet, S. J. and Carrasco, R. C. (2004), "A coupled elastoplastic damage model for geomaterials", *Comput. Methods Appl. Mech. Eng.,* **193**, 2625-2643.

Simo, J. C. and Ju, J. W. (1987), "Strain- and stress-based continuum damage models - I. Formulation", *Int. J. Solids Struct.,* **23**(7), 821-840.

Simone, A. and Sluys, L. (2004), "The use of displacement discontinuities in a rate-dependent medium", *Comput Methods Appl. Mech. Eng.*, **193**, 3015-3033.

Sluys, L. (1992), "Wave propagation, localisation and dispersion in softening solids", PhD Thesis, Delft University of Technology.

Sluys, L. J. and de Borst, R. (1996), "Failure in plain and reinforced concrete – an analysis of crack width and crack spacing", *Int. J. Solids Struct.,* **33**, 20-22, 3257-3276.

Strömberg, L. and Ristinmaa, M. (1996), "FE-formulation of nonlocal plasticity theory", *Comput. Methods Appl. Mech. Eng.* **136**, 127-144.

Tejchman, J. and Wu, W. (1993), "Numerical study on patterning of shear bands in a cosserat continuum", *Acta Mechanica*, **99**, 61-74.

Tejchman, J.. Herle, I. and Wehr, J. (1999), "FE-studies on the influence of initial density, pressure level and mean grain diameter on shear localisation", *Int. J. Num. Analytical Methods Geomech,* **23**(15), 2045-2074.

Tejchman, J. and Górski, J. (2007), "Deterministic and statistical size effect during shearing of granular layer within a micro-polar hypoplasticity", *Int. J. Num. Anal. Methods Geomech.* (in press).

den Uijl, J. A. and Bigaj, A. (1996), "A bond model for ribbed bars based on concrete confinement", *Heron* **41**, 201-226.

Walraven, J. C. (1978), "The influence of depth on the shear strength of lightweight concrete beams without shear reinforcement", TU-Delft Report 5-78-4, Delft University.

Walvaren, J. and Lehwalter, N. (1994), "Size effects in short beams loaded in shear", *ACI Struct. J.*, 585-593.

Wittmann, F. H., Mihashi, H. and Nomura, N. (1992), "Size effect on fracture energy using three-point bend tests", *Mater. Struct.,* **25**, 327-334.

Vervuurt, A., van Mier, J. G. M. and Schlangen, E. (1994), "Lattice model for analyzing steel-concrete interactions", *Comp. Methods and Advances in Geomechanics* (eds.: Siriwardane and Zaman), 713-718, Balkema, Rotterdam.

van Vliet, M. R. A. and van Mier, J. G.. M. (1996), "Experimental investigation of concrete fracture under uniaxial compression", *Mechanics of Cohesive-Frictional Materials*, **1**, 115-12.

CC